Implicit spatial averaging in inversion of inelastic x-ray scattering data

P. Abbamonte,[1] J. P. Reed,[1] Y. I. Joe,[1] Yu Gan,[1] and D. Casa[2]
[1]*Frederick Seitz Materials Research Laboratory and Department of Physics, University of Illinois, Urbana, Illinois 61801, USA*
[2]*Advanced Photon Source, Argonne National Laboratory, Argonne, Illinois 60439, USA*
(Received 13 April 2009; revised manuscript received 9 June 2009; published 4 August 2009)

Inelastic x-ray scattering (IXS) is now a widely used technique for studying the dynamics of electrons in condensed matter. We previously posed a solution to the phase problem for IXS [P. Abbamonte *et al.*, Phys. Rev. Lett. **92**, 237401 (2004)] that allows explicit reconstruction of the density propagator of a system. The propagator represents, physically, the response of the system to an idealized, point perturbation, so provides direct, real-time images of electron motion with attosecond time resolution and Å-scale spatial resolution. Here we show that the images generated by our procedure, as it was originally posed, are spatial averages over all source locations. Within an idealized, atomiclike model, we show that in most cases a simple relationship to the complete, unaveraged response can still be determined. We illustrate this concept for recent IXS measurements of single-crystal graphite.

DOI: 10.1103/PhysRevB.80.054302 PACS number(s): 78.70.Ck, 61.05.cc, 83.85.Hf

I. INTRODUCTION

Attoscience is an emerging discipline that exploits remarkable achievements in high harmonic generation (HHG) laser technology to study the dynamics of electrons in atoms, molecules, and condensed matter with subfemtosecond time resolution.[1–4] These advances have been paralleled by equally remarkable achievements in technology for x-ray experiments, both at the source and the endstation level. In particular, new approaches to inelastic x-ray scattering (IXS) provide a kinematic flexibility not previously accessible to energy-loss scattering techniques.[5]

We previously showed that if the nonresonant IXS cross section is sampled over a sufficiently broad range of momentum and energy, it can be inverted to explicitly reconstruct the density-density propagator of a material (the case of resonant IXS or "RIXS" will be discussed at the end of this article). The propagator, physically, represents the density induced in a medium by an idealized, point perturbation. Inversion therefore provides direct, real-time images of electron dynamics, with resolutions exceeding 20 as in time and 1 Å in space.[6] We have used this method, for example, to show that the valence exciton in LiF is a Frenkel exciton.[7]

This inversion method, as it was originally posed,[6] has a limitation: it makes use of only a subset of the full charge response of the material. To understand the origin of this limitation, recall that the (retarded) density propagator of a system is defined as

$$\chi(\mathbf{x}_1,\mathbf{x}_2,t) = -i/\hbar\langle g|[\hat{n}(\mathbf{x}_1,t),\hat{n}(\mathbf{x}_2,0)]|g\rangle\theta(t), \tag{1}$$

where $|g\rangle$ represents the ground state and $\hat{n}(\mathbf{x},t)$ is the many-body density operator

$$\hat{n}(\mathbf{x},t) = \hat{\psi}^\dagger(\mathbf{x},t)\hat{\psi}(\mathbf{x},t), \tag{2}$$

where $\hat{\psi}$ is a field operator for the interacting, Fermion system. Equation (1) represents the amplitude that a point disturbance in the electron density at location x_2 at time $t=0$ will propagate to point $\mathbf{x}_1$ at some later time t, so is a general measure of electron dynamics.

The two spatial coordinates, $\mathbf{x}_1$ and $\mathbf{x}_2$, are distinct. That is, the form of the response depends, in general, on the precise location of the source, $\mathbf{x}_2$ (on top of an atom versus between atoms, for example). The Fourier transform of the propagator is therefore a function of two momenta

$$\chi = \chi(\mathbf{k}_1,\mathbf{k}_2,\omega). \tag{3}$$

Unfortunately, in scattering there is only one momentum transfer, $\mathbf{k}$. IXS experiments do not measure all parts of the response in Eq. (3) but only its longitudinal (or "diagonal") components[8]

$$\chi(\mathbf{k},\omega) = \chi(\mathbf{k},-\mathbf{k},\omega). \tag{4}$$

This restricts the amount of information available with the IXS imaging approach. If the system is translationally invariant, this restriction poses no limits on the method. In a homogeneous system the propagator depends only on the difference $\mathbf{x}=\mathbf{x}_1-\mathbf{x}_2$, i.e.,

$$\chi(\mathbf{x}_1,\mathbf{x}_2,t) = \chi(\mathbf{x}_1-\mathbf{x}_2,t) \equiv \chi(\mathbf{x},t), \tag{5}$$

its Fourier transform is a function of only one momentum

$$\chi = \chi(\mathbf{k},\omega) \tag{6}$$

and IXS can provide a complete parameterization of the density propagator.

All real systems are made of atoms, however, so are never truly homogeneous. One can, nonetheless, carry out the inversion procedure described in Refs. 6 and 7 and construct detailed images of electron motion. But these images cannot be complete. Because they are based on a subset of all Fourier components of the response, the images must represent some kind of average of the complete response. For IXS inversion to be useful, it is necessary to articulate exactly what kind of average this is.

In this paper we show that the images produced in an IXS inversion correspond to the complete response, $\chi(\mathbf{x}_1,\mathbf{x}_2,t)$, averaged over all source locations, $\mathbf{x}_2$. In a homogeneous system, in which the response is independent of $\mathbf{x}_2$, the images can be considered complete. Even in an inhomogeneous

system, however, a simple physical picture is still applicable. We show, within a simple but illustrative model, that the overall size of the response scales with the electron density at the source location, $\mathbf{x}_2$. The average will, therefore, be dominated by source points of high electron density. We will show that, in cases of physical interest, the images will resemble closely the full response, $\chi(\mathbf{x}_1,\mathbf{x}_2,t)$, in which $\mathbf{x}_2$ coincides with the peak in the electron density. We discuss this conclusion in the context of some recent IXS studies of single-crystal graphite.

II. INVERSION OF IXS DATA

We begin by reviewing the mechanics of an IXS inversion. IXS measures the dynamic structure factor $S(\mathbf{k},\omega)$, defined as

$$S(\mathbf{k},\omega) = \sum_{i,f} |\langle f|\hat{n}(\mathbf{k})|i\rangle|^2 P_i \delta(\omega - \omega_f + \omega_i), \tag{7}$$

where $P_i = e^{-\beta\omega_i}/Z$ is the Boltzmann factor ($\beta = \hbar/kT$). The Fourier transform of S is a space-time correlation function for the density.[9] This correlation function, while interesting, is not causal so contains no direct information about dynamics.

$S(\mathbf{k},\omega)$ is, however, related to the charge propagator through the fluctuation-dissipation theorem

$$S(\mathbf{k},\omega) = \frac{1}{\pi}\frac{1}{1-e^{-\beta\omega}} Im[\chi(\mathbf{k},\omega)]. \tag{8}$$

The propagator χ is a truly causal quantity, so provides direct information about electron dynamics. Inverting this cross section, to reconstruct the propagator, requires four steps. The first is symmetrizing to convert from S to $Im[\chi]$. This is best done via the relationship[6]

$$Im[\chi(\mathbf{k},\omega)] = -\pi[S(\mathbf{k},\omega) - S(\mathbf{k},-\omega)] \tag{9}$$

which does not require exact knowledge of the temperature. Next, one must analytically continue the data. This can be done with simple, linear interpolation.[6,7] Third, one performs a sine transform of this imaginary part

$$\chi(\mathbf{k},t) = \int d\omega\, Im[\chi(\mathbf{k},\omega)]\sin\omega t, \tag{10}$$

where it is understood that $\chi(\mathbf{k},t)$ is zero for $t<0$. Equation (10) follows directly from the Kramers-Kronig relations and is the step in the procedure in which the phase is determined and causality is imposed. Finally, one performs a normal, Fourier transform of the spatial coordinates to get $\chi(\mathbf{x},t)$. This procedure has been used to image electronic motion in liquid water,[6] to show that the exciton in LiF is a Frenkel exciton,[7] and to study screening processes in graphite and graphene.[10,11]

III. IMPLICIT SPATIAL AVERAGING

We now stop to ask the following question: how do we interpret the output of this procedure for a system that does *not* have translational symmetry? If we carry out the procedure described in Sec. II, we will be left with a function of a single spatial variable, $\chi(\mathbf{x},t)$, which looks like the response of a homogeneous system. How should this function be interpreted?

To answer this question, we must determine an explicit relationship between this $\chi(\mathbf{x},t)$ and the complete response function $\chi(\mathbf{x}_1,\mathbf{x}_2,t)$. First, we write down the Fourier transform

$$\chi(\mathbf{x}_1,\mathbf{x}_2) = \int \frac{d\mathbf{k}_1 d\mathbf{k}_2}{(2\pi)^6}\chi(\mathbf{k}_1,\mathbf{k}_2)e^{i\mathbf{k}_1\cdot\mathbf{x}_1 + i\mathbf{k}_2\cdot\mathbf{x}_2}, \tag{11}$$

where the time dependence has been suppressed. Next, we recognize that if we insert the expression $g(\mathbf{k}_1,\mathbf{k}_2) = (2\pi)^3\delta(\mathbf{k}_1+\mathbf{k}_2)$ into the integrand

$$\chi(\mathbf{x}_1,\mathbf{x}_2) = \int \frac{d\mathbf{k}_1 d\mathbf{k}_2}{(2\pi)^6} g(\mathbf{k}_1,\mathbf{k}_2)\chi(\mathbf{k}_1,\mathbf{k}_2)e^{i\mathbf{k}_1\cdot\mathbf{x}_1 + i\mathbf{k}_2\cdot\mathbf{x}_2} \tag{12}$$

Eq. (11) reduces to

$$\chi(\mathbf{x}_1-\mathbf{x}_2) = \int \frac{d\mathbf{k}_1}{(2\pi)^3}\chi(\mathbf{k}_1,-\mathbf{k}_1)e^{i\mathbf{k}_1\cdot(\mathbf{x}_1-\mathbf{x}_2)}, \tag{13}$$

which we readily recognize to be the same as Eqs. (4) and (5). This means that one can think of $\chi(\mathbf{x},t)$ as the full function $\chi(\mathbf{x}_1,\mathbf{x}_2)$ having been Fourier filtered by the function $g(\mathbf{k}_1,\mathbf{k}_2)$.

A more physical interpretation can be achieved by applying the convolution theorem. The Fourier transform of g is given by

$$g(\mathbf{x}_1,\mathbf{x}_2) = \delta(\mathbf{x}_1-\mathbf{x}_2). \tag{14}$$

$\chi(\mathbf{x})$ is the Fourier transform of the product $g(\mathbf{k}_1,\mathbf{k}_2)\chi(\mathbf{k}_1,\mathbf{k}_2)$, which means it can be written as the convolution integral

$$\chi(\mathbf{x}_1-\mathbf{x}_2) = \int d\mathbf{x}_1' d\mathbf{x}_2' g(\mathbf{x}_1',\mathbf{x}_2')\chi(\mathbf{x}_1-\mathbf{x}_1',\mathbf{x}_2-\mathbf{x}_2') \tag{15}$$

$$= \int d\mathbf{x}_2'\chi(\mathbf{x}_1-\mathbf{x}_2',\mathbf{x}_2-\mathbf{x}_2'). \tag{16}$$

Redefining the origin and writing in terms of $\mathbf{x}=\mathbf{x}_1-\mathbf{x}_2$ we arrive at

$$\chi(\mathbf{x}) = \int d\mathbf{x}_2'\chi(\mathbf{x}+\mathbf{x}_2',\mathbf{x}_2'). \tag{17}$$

So, the physical meaning of $\chi(\mathbf{x},t)$ becomes quite clear. It is simply the complete susceptibility, $\chi(\mathbf{x}_1,\mathbf{x}_2,t)$, averaged over all possible source locations, $\mathbf{x}_2$. No such average is done in time, however, so $\chi(\mathbf{x},t)$ is still a direct probe of electron dynamics. Further, even in an inhomogeneous system, $\chi(\mathbf{x},t)$ provides detailed and direct insight into the dynamics of the system. To illustrate why, it is useful to examine a specific case.

IV. ONE ELECTRON IN A PERIODIC POTENTIAL

To illustrate the value of $\chi(\mathbf{x},t)$ for an inhomogeneous system, we consider the idealized case of a single electron

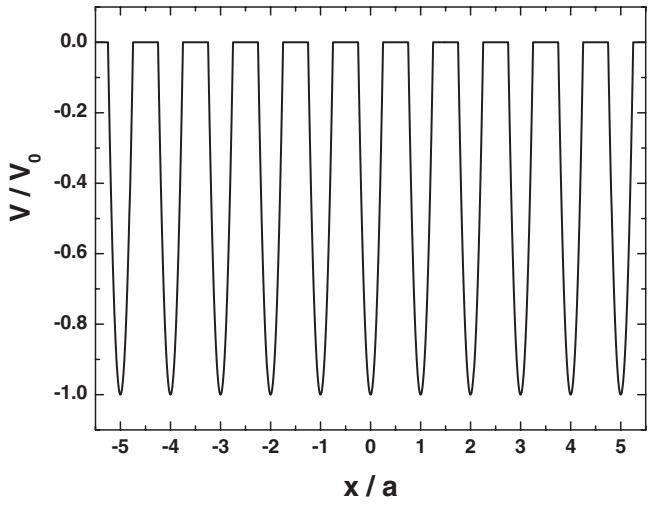

FIG. 1. Plot of the periodic array of potential wells described by Eqs. (18) and (19). For suitable choice of well depth and spacing, this system can be described in the tight-binding approximation as a set of coupled harmonic oscillators.

traveling in a one-dimensional periodic array of harmonic wells

$$V(x) = \sum_n v(x - na) \tag{18}$$

where each well is described by

$$v(x) = k(x^2 - r^2)\,\theta(r - |x|) \tag{19}$$

a being the distance between wells and r the radius of each well, as shown in Fig. 1 (the quantities x and k are now scalars). For sufficiently large values of k, the ground state of an isolated well will be a Gaussian

$$\phi(x) = \sqrt{2\pi\sigma}\,\exp - x^2/2\sigma^2 \tag{20}$$

with energy ω_0.

If the wells are weakly coupled the system can be described by a tight-binding model with hopping parameter t_h (to distinguish it from the time t). The eigenstates are then Bloch waves

$$\psi_k(x) = \sum_n \phi(x - na)e^{ikna} \tag{21}$$

and the energy level ω_0 will spread into a band with dispersion

$$\omega(k) = 2t_h[1 - \cos(ka)], \tag{22}$$

where we have shifted the zero of energy to coincide with the bottom of the band, i.e., $\omega(0)=0$.

We now wish to make an explicit comparison between the full response, $\chi(x_1,x_2,t)$ for this model, and the averaged response, $\chi(x,t)$. These quantities can be readily computed in one-electron Schrödinger theory but to keep the discussion general we will take a Green's function approach. The Fermion field operator for this system is

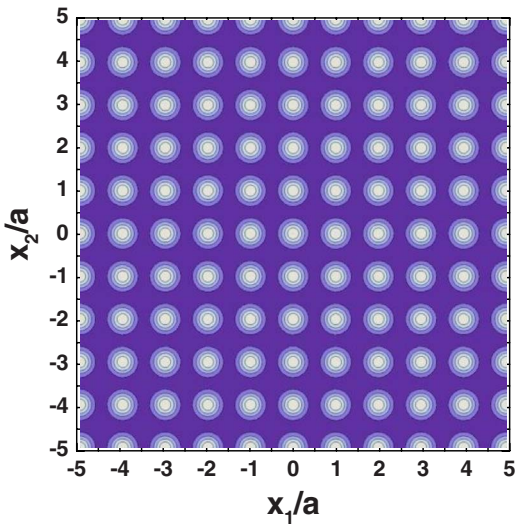

FIG. 2. (Color online) Contour plot of the prefactor $\psi_0(x_1)\psi_0(x_2)$ in Eq. (25).

$$\hat{\psi}(x,t) = \sum_k c_k \psi_k(x) e^{-i\omega(k)t}, \tag{23}$$

where c_k annihilates an electron with momentum k. Since we have only one electron, there is no need to specify the spin. In its ground state, the electron is at rest, i.e.,

$$|g\rangle = c_0^\dagger|0\rangle. \tag{24}$$

Plugging these definitions into the expression for the propagator, Eq. (1), we readily find

$$\chi(x_1,x_2,t) = \frac{8}{\pi}[\psi_0(x_1)\psi_0(x_2)] \times \left[\sum_{n_1,n_2} \phi(x_2 - n_2a)\phi(x_1 - n_1a)\cdot f_{n_2-n_1}(t)\right], \tag{25}$$

where

$$f_n(t) = \int_0^{\pi/a} dk\,\cos(kna)\sin\,\omega(k)t. \tag{26}$$

In general, the integral in Eq. (26) should exclude the value at $k=0$, however we may include it since $\sin\,\omega(0)t=0$. Note that $f_n(t)=f_{-n}(t)$.

The propagator, Eq. (25), consists of two factors, which can be thought of as propagators for the individual electron and hole. The first factor

$$\psi_0(x_1)\psi_0(x_2) \tag{27}$$

is independent of time and has a strong dependence on x_2. We plot this factor in Fig. 2, where we have chosen $\sigma=a/5$. We see that this factor is strongly dependent on x_2, its maximum possible value being reached when x_2 resides at the center of a well, i.e., the peak of the ground-state probability density.

We now evaluate Eq. (25) and examine the properties of the full propagator. For this purpose we evaluated $f_n(t)$, out

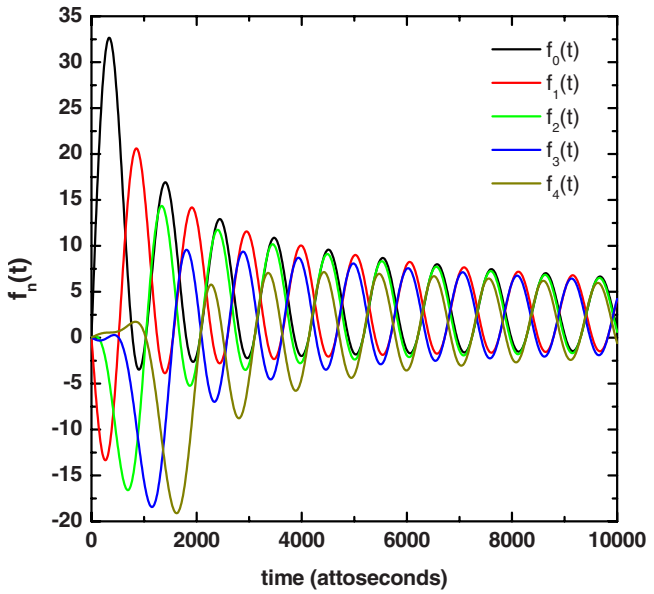

FIG. 3. (Color online) Plots of the function $f_n(t)$ for values of n out to fourth neighbors. Energy rapidly spreads from the first Wigner-Seitz cell ($n=0$) into neighboring cells.

to $n=5$ (fifth neighbors), using the value $t_h=1$ eV. The results are shown in Fig. 3. The resulting $\chi(x_1,x_2,t)$ is shown as a contour plot, in Fig. 4, as a function of x_1 and t, for the specific values $x_2=0$ (the source in the center of a well) and $x_2=a/2$ (source half way between two wells). In accordance with the physical meaning of a propagator, at $t=0$ the system appears to be struck by an instantaneous charged perturbation, setting up a disturbance in the electron-probability density. As time progresses the disturbance propagates away from the source location, dispersing through the lattice in a manner dictated by the dispersion of the band [Eq. (22)].

When $x_2=0$, the disturbance is symmetric around $x_1=0$ and has a distinct temporal periodicity determined by the bandwidth. When $x_2=a/2$, on the other hand, the disturbance is asymmetric and no longer has a clear temporal periodicity. These two cases are distinctly different, and illustrate how local field effects, arising from broken translational symmetry, affect the response properties of an atomiclike system.

Most importantly, in Fig. 4(c) we compare, on a linear plot, the two quantities $\chi(x_1,0,t)$ and $\chi(x_1,a/2,t)$ at a time $t=1000$ as. Notice that the $x_2=0$ case is larger than the $x_2=a/2$ case by a factor of ~ 200. This is partly a result of the prefactor Eq. (27) and has the physical meaning that the system responds more strongly if it is "struck" at a region of higher electron-probability density.

We now consider the averaged quantity, $\chi(x,t)$, which was determined by evaluating Eq. (17), i.e., by integrating images like those shown in Figs. 4(a) and 4(b) for x_2 values between $-a/2$ to $a/2$. The result is shown in Fig. 5. Remarkably, it is visually indistinguishable from Fig. 4(a).

The reason these two plots look the same is that $\chi(x_1,x_2,t)$ is bigger when x_2 coincides with the center of a well. So the average, Eq. (17), is dominated by its contribution from $x_2\sim 0$, resulting in a close resemblance to Fig. 4(a). In other words, the averaged quantity $\chi(x,t)$, to a reasonable approximation, can be thought of as the complete

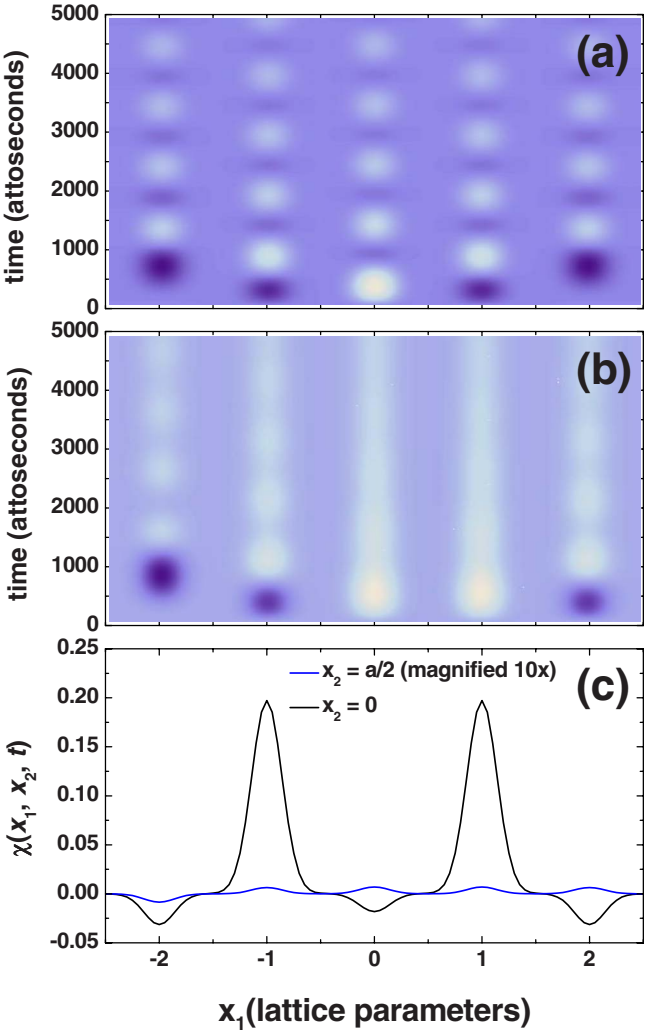

FIG. 4. (Color online) (a) Contour plot of $\chi(x_1,x_2,t)$ for $x_2=0$, i.e., for the source located in the center of an "atom". The disturbance created is symmetric around the source point and propagates at the average group velocity of the band. (b) Same plot, but with $x_2=a/2$, i.e., for the source half way in between two atoms. The disturbance is now asymmetric, and no longer oscillates with a well-defined period. (c) Sections through the plots in (a) and (b) at $t=1000$ as on a linear plot, showing that the magnitude of the response in (a) is larger by ~ 100 times.

response $\chi(x_1,x_2,t)$ for x_2 residing at the peak in the electron probability density.

This illustration was for the extremely simplistic case of one electron in an array of wells. However the result should be quite general and apply also to a many-electron system in the presence of strong interactions. The size of the propagator is determined by the expectation value of the product of two many-body operators, $\hat{n}(\mathbf{x}_1,t)\cdot\hat{n}(\mathbf{x}_2,0)$. The upper bound on this quantity is set by the product of their expectation values, $\langle\hat{n}(\mathbf{x}_1,t)\rangle\cdot\langle\hat{n}(\mathbf{x}_2,0)\rangle$. The propagator will therefore always have a tendency to be larger when $\mathbf{x}_1$ and $\mathbf{x}_2$ individually reside in regions of higher electron density. In particular, collective modes of the density, such as plasmons and phonons, which are most easily studied with IXS, should generally have this property.

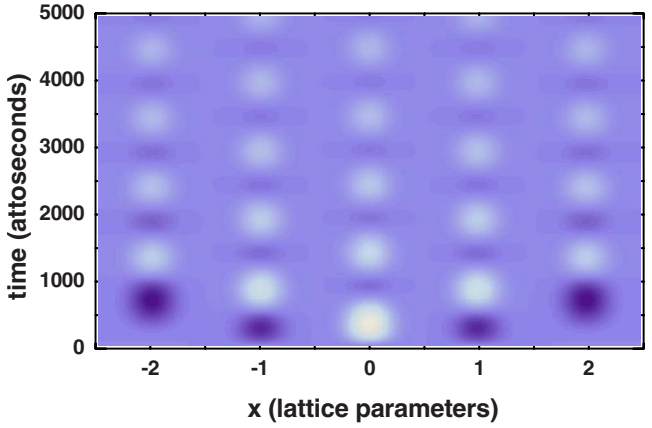

FIG. 5. (Color online) $\chi(x_1,x_2,t)$ averaged over all source locations, x_2. This is the image that would result by inverting IXS data. Note the close similarity to Fig. 4(a).

V. EXAMPLE: SINGLE CRYSTAL GRAPHITE

To illustrate how this concept can be useful for understanding experimental data, we briefly consider the real example of single-crystal graphite. Graphite is a layered structure comprising an *abab*-type stacking of graphene sheets. The sheets have a honeycomb structure with two distinct C sites, which are related by a translation combined with a 60° rotation of the coordinates.

We performed IXS measurements on a commercially obtained single crystal (not highly oriented pyrolytic graphite) of graphite. The experiments were done at Sector 9 XOR of the Advanced Photon Source. The details of this experiment are being published in two separate articles.[10,11] In brief, spectra were taken at medium energy resolution ($\Delta E \sim 300$ meV) for $\mathbf{k}$ vectors spanning the entire basal plane, allowing a spatially two-dimensional reconstruction of the translationally averaged propagator $\chi(x,y,t)$, which is shown in Fig. 6 for a time slice of $t=400$ as. The image exhibits a pronounced sixfold symmetry, which is an unsurprising result of the underlying hexagonal symmetry of the lattice.

Our result from Sec. IV, i.e., that χ is largest when the source is at the density maximum, provides a different way of thinking about this sixfold symmetry. The ground-state electron density of graphite is maximum at the center of a C atom, each of which sits at a location with threefold local symmetry. We expect that Fig. 6 will resemble the full $\chi(\mathbf{x}_1,\mathbf{x}_2,t)$, for the specific case of $\mathbf{x}_2$ centered on a C site. In accordance with the local environment, χ should also exhibit threefold symmetry.

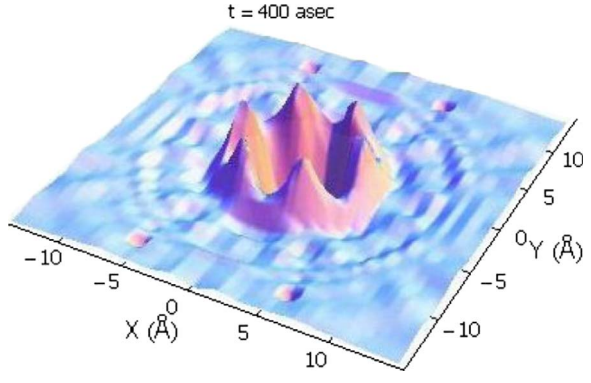

FIG. 6. (Color online) $\chi(x,y,t)$ for a real IXS experiment from a single crystal of graphite. The sixfold symmetry is a result of the underlying honeycomb symmetry of the graphene sheets. This image can be thought of as a superposition of two sources, one on the center of a C atom in each of the crystalline sublattices (see text).

There are, however, two distinct C atoms in a unit cell with the same ground-state electron density. By Eq. (17), the averaged response in Fig. 6 should be a *coherent* superposition of sources at these two distinct C locations. Further, though each C atom locally has only threefold symmetry, one is rotated 60° from the other. When the two are superposed, the sixfold symmetry in Fig. 6 results.

Our goal here is not to explain the existence of sixfold symmetry in graphite, which was never a mystery. The point is that Eq. (17) provides a useful, conceptual framework for relating the spatially averaged response deduced from IXS data to the complete, unaveraged response.

VI. DISCUSSION

It may be possible to extend IXS inversion methods to image more than just an average response. Many years ago it was shown[12,13] that by setting up a standing wave in a material, for example, by hitting a Bragg reflection, one can measure a subclass of the off-diagonal components of the susceptibility. Under standing-wave conditions, the initial photon will be in a superposition of two different momentum eigenstates, in which case the IXS cross section will contain contributions from $\chi(\mathbf{k}_1,\mathbf{k}_2,\omega)$, where $\mathbf{k}_1 \neq -\mathbf{k}_2$. In principle this method can be used to "anchor the problem" in space and potentially reconstruct the complete $\chi(\mathbf{x}_1,\mathbf{x}_2,t)$. Whether it is experimentally possible to measure a sufficiently large set of these off-diagonal terms is a subject of current investigation.

The reader should be aware that our method for inverting IXS data works only for nonresonant inelastic x-ray scattering, i.e., in which the beam energy is kept far from any core absorption edge. In this case the cross section is proportional to $S(\mathbf{k},\omega)$, which is related to the propagator.[9] For the case of RIXS, in which the beam energy is tuned to an edge (in the soft x-ray range, for example), the scattering proceeds through interference among a continuum intermediate states. The RIXS cross-section explicitly depends on both the incoming and outgoing photon energies (and momenta), rather than just their difference.[9] In this case the scattering cannot be trivially related to any causal, response function, and explicit visualization of the dynamics is not possible. Various scenarios for mapping the RIXS cross section onto a response function, by integrating out the intermediate states, have been proposed.[14–16] If one of these approaches proves viable, our method could be applied to RIXS as well.

The reader familiar with Compton scattering may wonder whether there is a relationship between our $\chi(\mathbf{x},t)$ and the auxiliary function $B(\mathbf{x})$ used in the Debye-Bessel method for extracting a two-dimensional momentum-density profile from a set of one-dimensional Compton scattering measurements.[17,18] The relationship, if any, is extremely in-

direct. To begin, the quantity B is only definable in one-electron band theory, where it is assumed the ground state is a single Slater determinant of occupied, one-electron Bloch states. The cross section is assumed to depend only on these occupied levels, the recoiling electron having been treated as a plane wave and mapped out of the problem. B is therefore related to the one-electron Green's function, and is more closely related to one-electron probes, such as ARPES than it is to standard IXS.

Like $\chi(\mathbf{x},t)$, $B(\mathbf{x})$ is a function of only one spatial variable. However it is not a spatial average. $B(\mathbf{x})$ is actually an autocorrelation or, more precisely, a coherent sum of the autocorrelations of each of the individual, occupied Bloch levels. An autocorrelation function is an extremely useful quantity, particularly for uncovering hidden periodicities,[19] and has been exploited in algorithms to reconstruct Fermi surfaces from Compton data.[17] However, the arguments we make in this article do not apply to B in any obvious way.

In summary, we have shown that IXS imaging, as prescribed in Ref. 6, provides images of the charge propagator, $\chi(\mathbf{x}_1,\mathbf{x}_2,t)$, that are averaged over all source locations, $\mathbf{x}_2$. No such average is done in time, however, so this method is still a *direct* probe of electron dynamics in the attosecond regime. The size of the propagator is much larger when $\mathbf{x}_2$ resides in a region of high density, so one can think of the averaged images as corresponding to the complete response, for $\mathbf{x}_2$ residing at the peak of the electron density. Standing wave methods, in which the incident photon is placed in a superposition of momenta, may extend the applicability of the technique.

ACKNOWLEDGMENTS

We thank David Cahill, Gerard C. L. Wong, and Robert Coridan for helpful discussions, and Xiaoqian Zhang for a careful reading of the manuscript. This work was funded by the Materials Sciences and Engineering Division, Office of Basic Energy Sciences, U.S. Department of Energy under Grant No. DE-FG02-07ER46459. Use of the Advanced Photon Source was supported by DOE under Contract No. DE-AC02-06CH11357.

[1] P. H. Bucksbaum, Science **317**, 766 (2007).
[2] T. Brabec, Phys. World **17** (11), 29 (2004).
[3] H. Kapteyn, O. Cohen, I. Christov, and M. Murnane, Science **317**, 775 (2007).
[4] F. Krausz and M. Ivanov, Rev. Mod. Phys. **81**, 163 (2009).
[5] W. Schülke, *Electron Dynamics by Inelastic X-Ray Scattering* (Oxford University Press, Oxford, U.K., 2007).
[6] P. Abbamonte, K. D. Finkelstein, M. D. Collins, and S. M. Gruner, Phys. Rev. Lett. **92**, 237401 (2004).
[7] P. Abbamonte, T. Graber, J. P. Reed, S. Smadici, C.-L. Yeh, A. Shukla, J.-P. Rueff, and W. Ku, Proc. Natl. Acad. Sci. U.S.A. **105**, 12159 (2008).
[8] IXS measures, of course, only the imaginary part $\mathrm{Im}[\chi(k,-k,\omega)]$, but the real part can be retrieved by Kramers-Kronig transform.
[9] S. K. Sinha, J. Phys.: Condens. Matter **13**, 7511 (2001).
[10] B. Uchoa, J. P. Reed, Y. I. Joe, D. Casa, E. Fradkin, Y. Cai, and P. Abbamonte (unpublished).
[11] J. P. Reed, B. Uchoa, Y. I. Joe, D. Casa, E. Fradkin, Y. Cai, and P. Abbamonte (unpublished).
[12] W. Schülke, Phys. Lett. **83A**, 451 (1981).
[13] J. A. Golovchenko, D. R. Kaplan, B. Kincaid, R. Levesque, A. Meixner, M. F. Robbins, and J. Felsteiner, Phys. Rev. Lett. **46**, 1454 (1981).
[14] J. van den Brink and M. van Veenendaal, J. Phys. Chem. Solids **66**, 2145 (2005).
[15] A. Kotani and S. Shin, Rev. Mod. Phys. **73**, 203 (2001).
[16] P. Abbamonte, C. A. Burns, E. D. Isaacs, P. M. Platzman, L. L. Miller, S. W. Cheong, and M. V. Klein, Phys. Rev. Lett. **83**, 860 (1999).
[17] I. Matsumoto, J. Kwiatkowska, F. Maniawski, M. Itou, H. Kawata, N. Shiotani, S. Kaprzyk, P. E. Mijnarends, B. Barbiellini, and A. Bansil, Phys. Rev. B **64**, 045121 (2001).
[18] M. Cooper, P. E. Mijnarends, N. Shiotani, N. Sakai, and A. Bansil, *Ray Compton Scattering* (Oxford University Press, Oxford, U.K., 2004).
[19] E. D. Isaacs, A. Shukla, P. M. Platzman, D. R. Hamann, B. Barbiellini, and C. A. Tulk, Phys. Rev. Lett. **82**, 600 (1999).